Supplemental Information

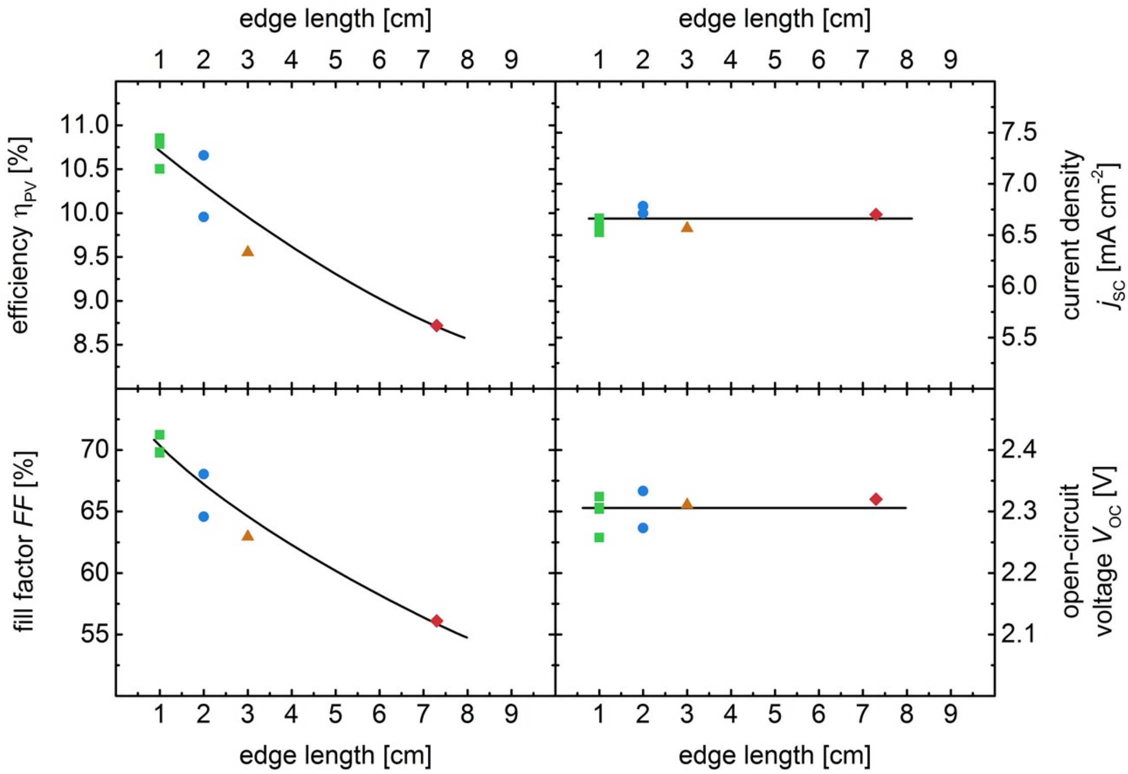

Figure S1. Efficiency η_{PV}, fill factor *FF*, open-circuit voltage V_{oc}, and short-circuit current density j_{sc} of a-Si:H/a-Si:H/μc-Si:H tandem solar cells with different edge lengths/areas. The parameters were extracted from the *j*-*V* curves partially plotted in Fig. 1. The solid lines were plotted as a guide to the eye. A longer edge length (larger solar cell area) leads to a significant reduction of the *FF* while j_{sc} and V_{oc} are maintained. The loss in *FF* is a result of the increased series resistance of the solar cell that is introduced by the longer distance the charge carriers have to travel through the TCO and the higher current of the larger cell. Ultimately, this leads to a reduced efficiency for larger solar cells.

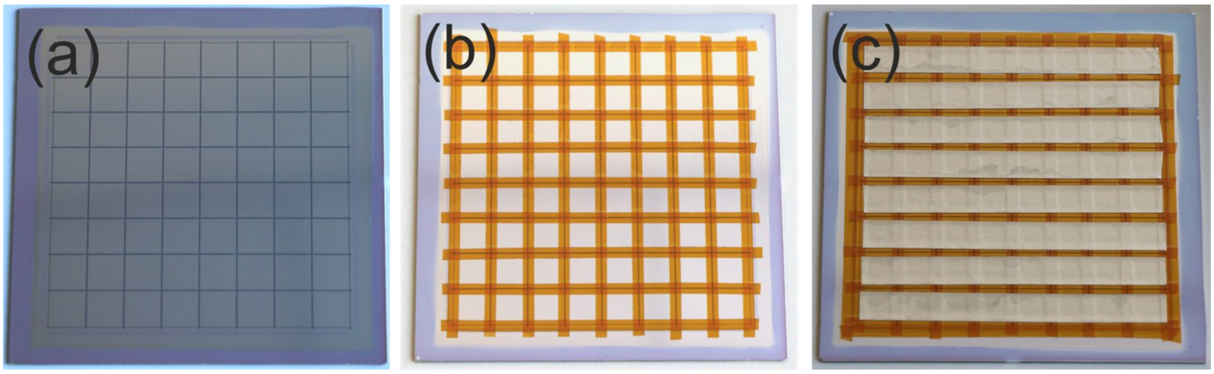

Figure S2. Photographs of the laser scribed large area solar cell from the rear side after (a) the second laser processing step LP2 (step iv in Fig. 1b), (b) insulation of the front and rear contact areas (step v in Fig. 1b), and (c) during parallel connection of the individual 1 × 1 cm^2 solar cells to one large 8 × 8 cm^2 solar cell (step vi in Fig. 1b).

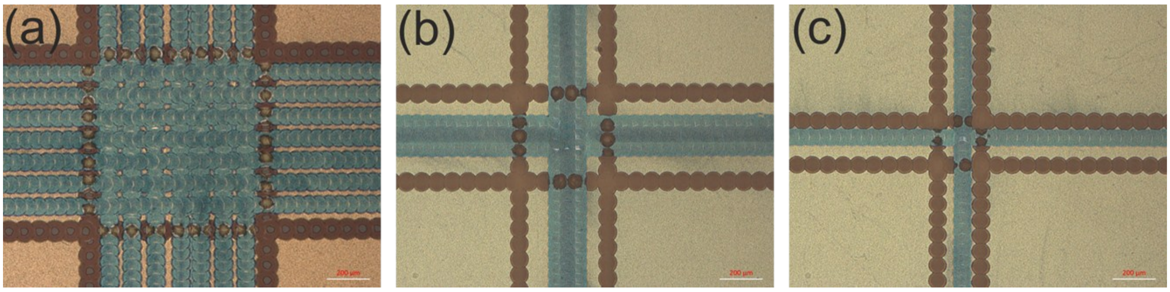

Figure S3. Micrographs of laser scribed front contact grids with (a) 800 µm, (b) 400 µm, and (c) 200 µm contact width, which correspond to 14%, 7%, and 3.5% active area loss, respectively.

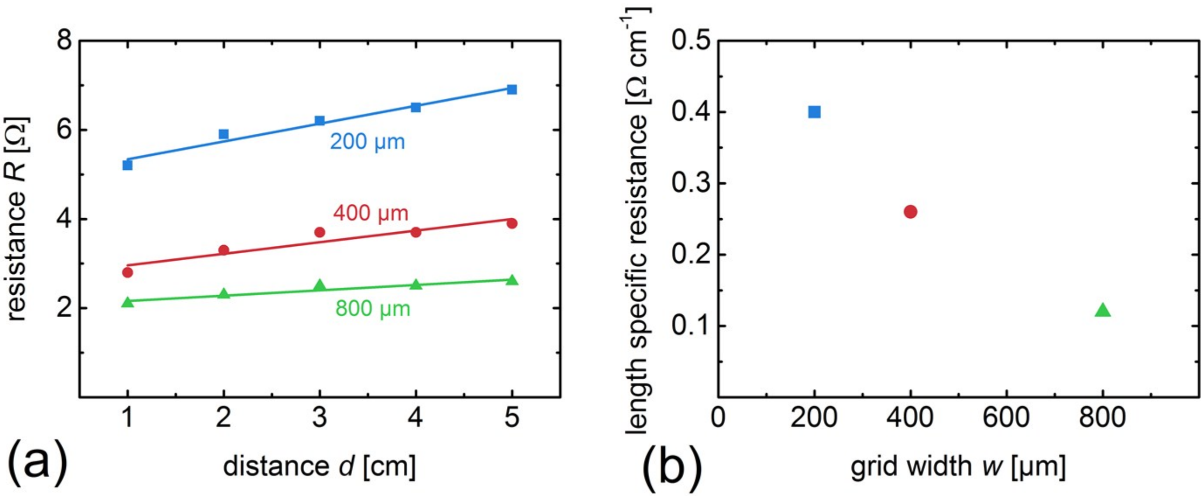

Figure S4. (a) Resistances measured along laser patterned front contact grids with 200 µm, 400 µm, and 800 µm finger width using a four-point probe plotted versus the distance along the gridlines. The slope of the linear fit corresponds to the length specific resistance plotted in (b). It decreases with increasing finger width. However, a significant effect in the solar cell performance was not observed. Thus, the series resistance of the front contact metal grid with 200 µm finger width is sufficiently small to maintain efficient charge carrier collection. This is in agreement with the comparable performance of the large solar cell in Fig. 3 and the small solar cells.

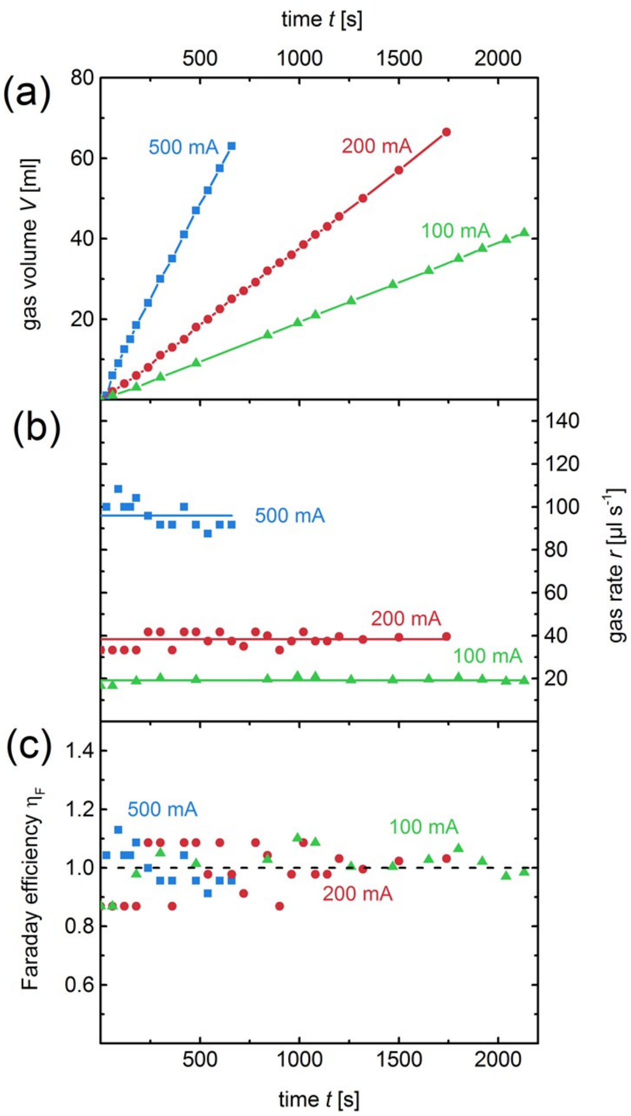

Figure S5. (a) Collected total gas volume during galvanostatic electrolysis at 100 mA, 200 mA, and 500 mA in an EC cell featuring Ni electrodes for both anode and cathode in 1 M KOH. No membrane was applied and the hydrogen and oxygen gases were collected together in one inverted burette for quantification. (b) Gas rates corresponding to the collected gas volumes for the different currents applied. The dots represent the gas rates determined from the collected gas and the solid lines correspond to the expected gas rate calculated via Faraday's law of electrolysis for the applied currents. The good agreement between calculated and measured gas rates point to a Faraday efficiency of unity. This is also apparent from (c). Here, the ratio between expected and measured gas rates is plotted, which corresponds to the Faraday efficiency. The values scatter around a value of 1. Thus, under realistic conditions the system is proven gas tight and no significant side reactions take place.

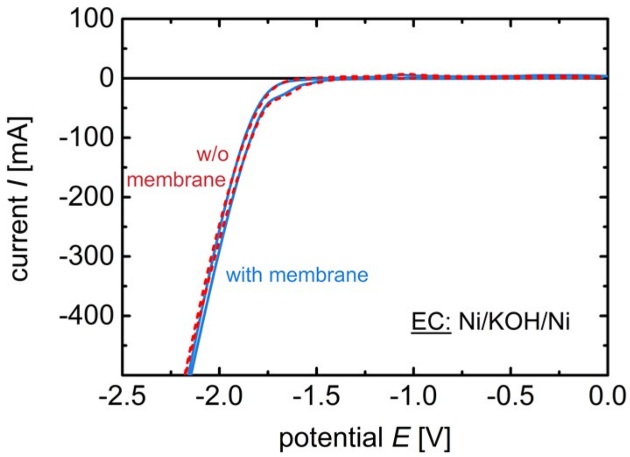

Figure S6. Cyclic voltammograms of the EC cell employing Ni electrodes for both anode and cathode in 1 M KOH with and without an anion exchange membrane to separate the half cells. Only a minor increase of the slope was observed when the membrane was introduced which may correspond to a slight increase of the system's series resistance. The very similar behavior suggests that the membrane does not significantly impact the performance of the electrolysis cell.

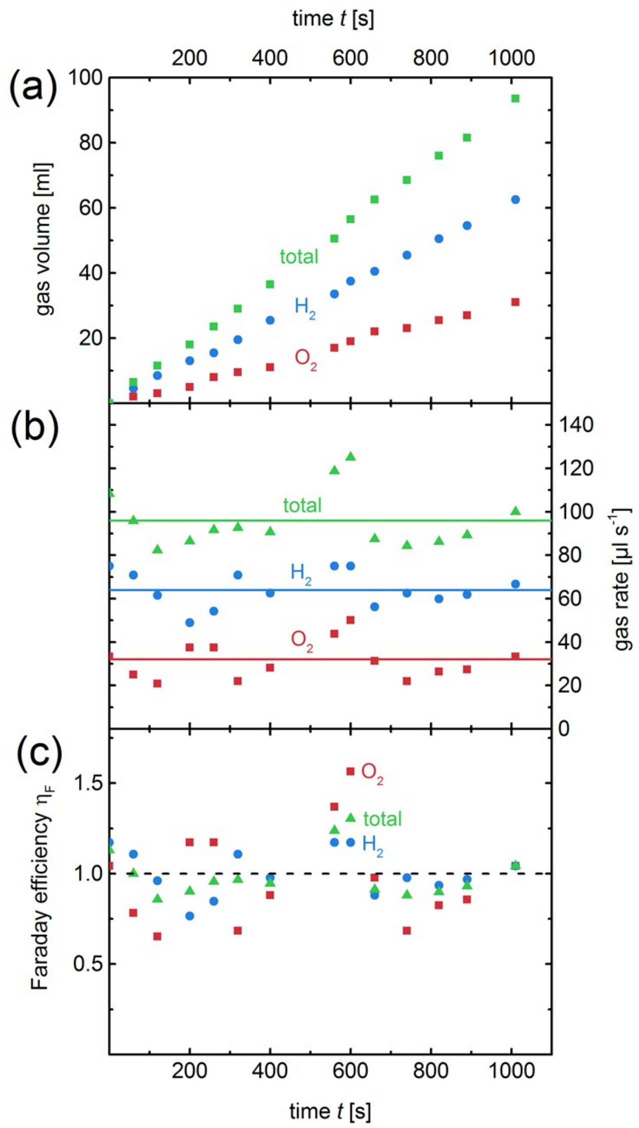

Figure S7. (a) Collected hydrogen and oxygen gas volumes during galvanostatic electrolysis at 500 mA in an EC cell featuring Ni electrodes for both anode and cathode in 1 M KOH. An anion exchange membrane was applied and the hydrogen and oxygen gases were collected in two separate inverted burettes for quantification. Additionally, the sum of both gas volumes is plotted. (b) Gas rates corresponding to the collected hydrogen and oxygen gas volumes. The dots represent the gas rates determined from the collected gas and the solid lines correspond to the expected gas rate calculated via Faraday's law of electrolysis for the applied current. Again, the gas total gas rate is given which was calculated as the sum of the individual gas rates. The ratio between hydrogen and oxygen was approximately two. (c) The Faraday efficiency calculated as the ratio between expected and measured gas rates. The values scatter around a value of 1. Thus, under realistic conditions the system is proven gas tight and no significant side reactions take place. Furthermore, cross contamination of the gases is expected to be small due to the hydrogen/oxygen ratio of two.

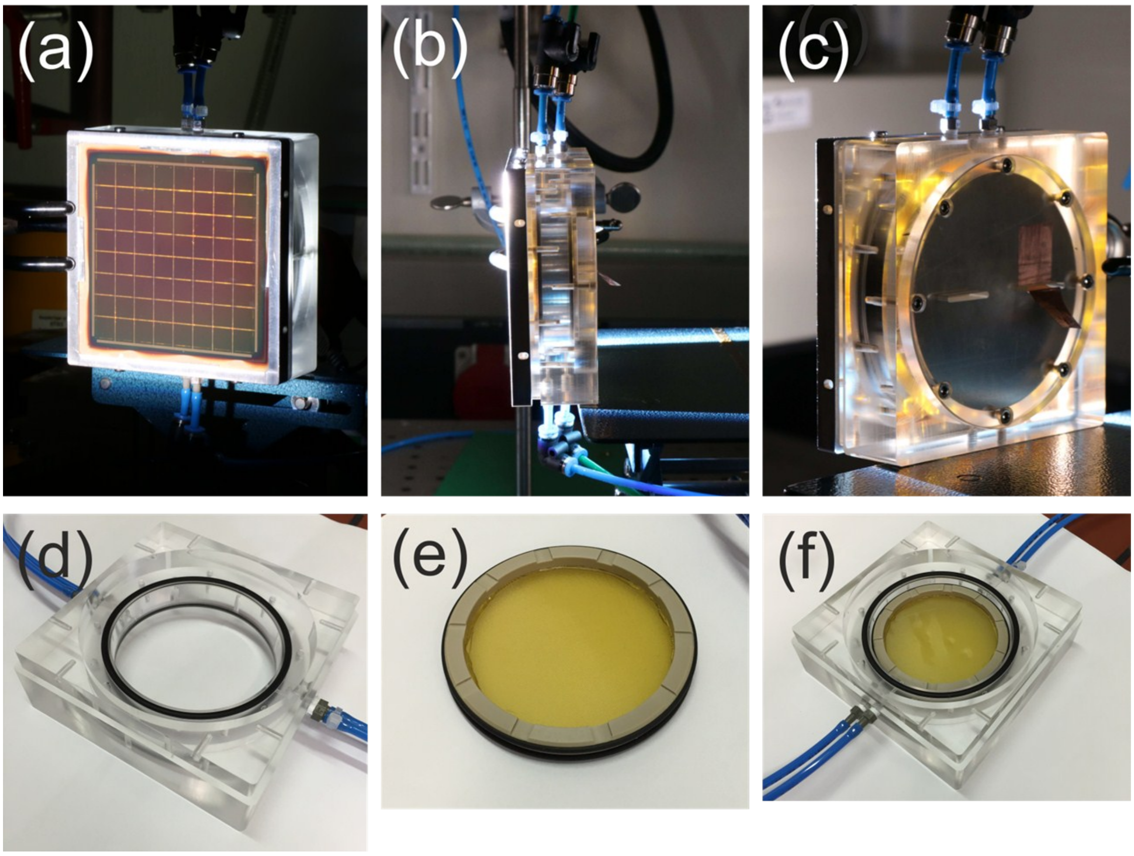

Figure S8. Photographs of the modular PV-EC setup with an electrode distance of 11 mm. (a) Front side with laser patterned 8 × 8 cm^2 solar cell, (b) side view of the module without membrane, (c) rear side of the module with round Ni electrode, (d) PMMA reactor body with O-ring seals, (e) ring with anion exchange membrane, (f) PMMA reactor with mounted anion exchange membrane.